Advanced monolithic arrays of Silicon Drift Detectors for elemental mapping applications

R. Alberti, S. Buzzetti, C. Fiorini, C. Guazzoni, T. Klatka
Politecnico di Milano, Dipartimento di Elettronica e Informazione, 20133 Milano, Italy and INFN, Sezione di Milano, Italy

P. Lechner
PN Sensor GmbH, Roemer Strasse 28, München D-80803, Germany

A. Longoni
Politecnico di Milano, Dipartimento di Elettronica e Informazione, 20133 Milano, Italy, INFN, Sezione di Milano, Italy and IFN-CNR, Sezione di Milano

L. Strüder
Max Planck Institut für Extraterrestriche Physik, Otto-Hahn-Ring 6, München D-81739, Germany

Recent technological developments and new topology designs made Semiconductor Drift Detectors ideal devices for high-resolution X-ray spectroscopy. In this paper we present advanced monolithic arrays of Silicon Drift Detectors suitable for elemental mapping applications. The main features of the designed arrays together with the summary of their performance are discussed. The measured average resolution is about 140 eV FWHM at the Mn Kα line at 1 μs shaping time. Up to 300 kcps the resolution stays below 220eV FWHM with 375 ns shaping time. Few examples of elemental mapping in geology, archeometry, and chemical analyses are reported.

1. INTRODUCTION

In the field of X-ray spectroscopy high energy resolution and low energy detection capability are basic requirements. The energy resolution of a detection system depends both on the intrinsic resolution of the detector and on the electronic noise of the system. The intrinsic resolution of the detector depends on the statistical fluctuations related to the conversion mechanism and sets a lower limit to the achievable resolution. The noise added by the readout electronics depends both on the detector characteristics (leakage current and output capacitance) and on the characteristics of the front-end electronics. In order to improve the achievable energy resolution, the detector capacitance and the stray capacitances connected to the output node should be minimized. Moreover the input capacitance of the front-end electronics should be "matched" to the detector capacitance.

Recent technological developments and new topology designs made Semiconductor Drift Detectors (SDDs) ideal devices for high-resolution X-ray spectroscopy. The Semiconductor Drift Detector [1], invented by E. Gatti and P. Rehak in 1983, is characterized by low output capacitance (of the order of 100 fF), independent of the active area. The SDD, due to its very small output capacitance, can reach energy resolutions approaching the ones of liquid nitrogen cooled detectors, with the advantage of a much shorter shaping time (shorter than 1 μs) [2].

The subdivision of the total active area in several independent detectors allows the increase of the maximum counting rate of the system with respect to a single detector of the same total active area. The particular structure of the detector array allows the transport of the X-ray excitation beam to the sample through the hole in the center of the array, thus optimizing the solid angle for the collection of the X-ray fluorescence. All these features guarantee high performances in terms of energy resolution and maximum count rate.

2. STATE-OF-THE ART 12 ELEMENT RING-SHAPED ARRAY

2.1. Silicon Drift Detector working principle

Fig. 1 shows the scheme of principle of a single-element Silicon Drift Detector (SDD) [1, 3]. The symmetry of the detector is radial, with a structure composed of p+ concentric rings implanted on the front side of the device. A continuous p+ junction implanted on the backside of the detector acts as radiation entrance window. A careful tailoring of the shallow implantation of the p+ back electrode guarantees an effective 'dead' layer at the entrance window smaller than 150 Å, giving a quantum efficiency higher than 80% at the carbon Kα line (277 eV) [4]. At high energy, the X-ray detection efficiency, limited by the total thickness of the device is higher than 90% at 10 keV, 30% at 18 keV and 14% at 26 keV (300 μm thickness). The increase of the detector thickness to 450

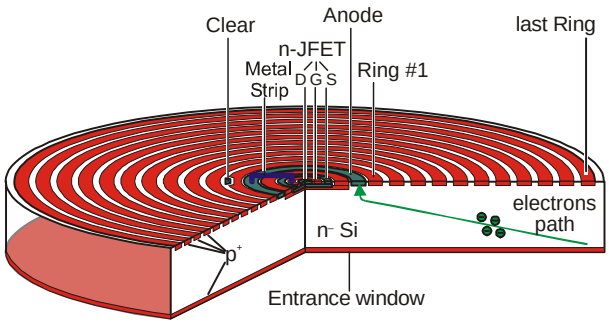

Figure 1. Architecture of a SDD especially designed for X-ray spectroscopy.

μm improves the quantum efficiency to about 45% at 18keV and 18% at 26keV.

To take full advantage of the intrinsic low output capacitance of the SDD, the input JFET of the 'front-end' electronics has been integrated in the central region of the detector, with the gate connected to the anode by means of a metal strip. In this way a correct capacitive matching between the detector and the first stage of amplification is achieved and the stray capacitances of the connections are minimized. This solution has also the advantage to reduce the sensitivity of the detector to microphonic noise. The integrated transistor is a non-conventional n-channel JFET, designed to be operated on fully depleted high resistivity silicon.

2.2. 12-element Silicon Drift Detector array

The monolithic detector array whose layout is shown in Figure 2 is composed of 12 independent SDDs, each one with an active area of 5 mm^2 [5]. The starting material is a 300 μm-thick high resistivity (2 kΩ cm) silicon substrate. Each SDD of the array has the input JFET of the readout electronics directly integrated in close proximity of the collecting anode to reach optimum performance. The hole in the center of the array has been laser cut. In order to avoid any undesired effect due to laser cutting the region around the central hole is isolated from the detector bulk by a specially designed guard ring structure. No increase of the detector's leakage current has been observed after the laser cut. Guard rings surround also the active region of the array toward the external border of the chip. The working temperature of the array is about –10°C, which is easily obtained with a Peltier cooler.

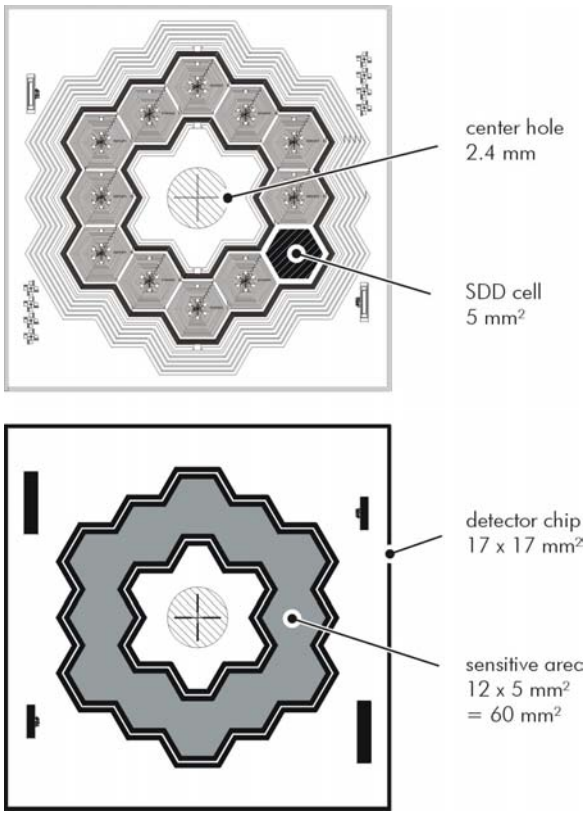

Figure 2. Layout plot of the 12-channel SDD with the central hole. The upper plot shows the detector front side with the drift ring structures and the integrated readout electronics. The lower plot shows the detector back side with the unstructured radiation entrance window.

Fig. 3 shows the achieved energy resolution at the Mn Kα line (5.9 keV). The average value is 172.7 eV FWHM (Gaussian fitting). The specified values of the measured FWHM demonstrate the high degree of homogeneity in the response of the individual detector cells. The obtained energy resolution is within the range known for the single unit SDDs proving that the properties of one detector cell do not 'suffer' from the integration in a multi-cell SDD.

3. THE NOVEL FOUR-ELEMENT RING-SHAPED HIGH-RESOLUTION SILICON DRIFT DETECTOR

3.1. 4-element detector design

Fig. 4 shows the layout of the novel ring-shaped detector constituted by a monolithic array of 4 SDDs of the new "Droplet"-type designed for high-resolution, high-rate X-ray spectroscopy. Guard rings surround the central hole and the periphery of the active area to prevent leakage current injection from the undepleted regions inside the active area. The location of the collecting anode (shown as a black dot in Figure 4) of each SDD away from the center of the active region allows the reduction of the anode dimensions. In fact, differently from the previous arrays

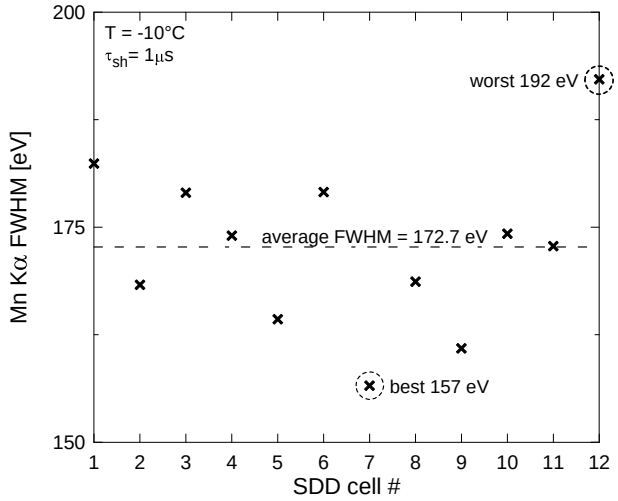

Figure 3. Energy resolution at each detector cell measured as the FWHM at the Mn Kα line when irradiating the detector with a ^{55}Fe radioactive source. During the spectroscopic test all detector cells are biased and active and connected to the DAQ.

thanks to the asymmetry of the arrival path of the signal charge, the front end JFET can be integrated outside the anode. Consequently, the anode capacitance of the "droplet" type SDDs is lower than that of the conventional type. The total capacitance at the transistor gate (anode, gate and stray capacitances) is of the order of 120 fF, to be compared with the 230 fF output capacitance of a conventional SDD [6]. The energy resolution is consequently improved. Moreover, this geometry allows an easy screening of the anode and transistor regions by means of a collimator, with a consequent improvement of the peak-to-valley ratio in the collected spectrum. The total active area of the 4-element detector is about 60 mm^2 (15 mm^2 per detector element) and it reduces to about 50 mm^2 by screening the anode and transistor regions. The detector thickness is 450 μm, thus improving the detector quantum efficiency. The subdivision of the area in four independent detectors increases the maximum counting rate of the system with respect to a single detector with the same area.

3.2. 4-element detector performances

References [7,8] report the results of the deep characterization of the novel four-element detector. Here we summarize the relevant results showing the main detector performances. Figure 5 shows the energy spectra collected by the four elements without any collimation when the detector was irradiated with a ^{55}Fe radioactive source. The detector was Peltier cooled at –20°C and the average count rate was about 2 kHz. The measured average resolution is about 140 eV FWHM at the Mn Kα line at 1 μs shaping time. Up to 300 kcps the resolution stays below 220eV FWHM with 375 ns shaping time. Better performances will be achieved with the front-end electronics in charge amplifier configuration with pulsed reset. A peak-to-background ratio (defined as the ratio between the peak value of the Mn Kα line and the average value of the shoulder evaluated between 800 eV and 1200 eV) of the order of 6000 has been obtained with a beam collimation of 500μm.

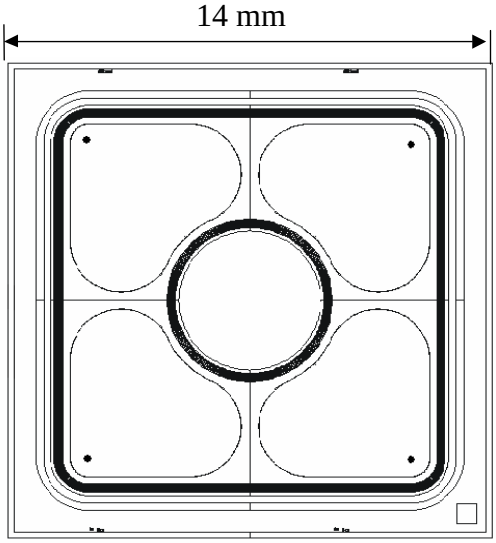

Figure 4. Schematic layout of the novel ring-shaped 4-channel SDD Droplet detector.

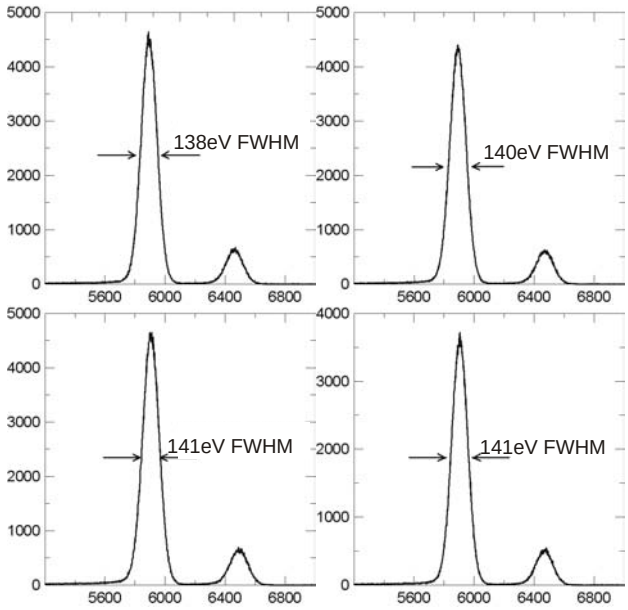

Figure 5. Energy spectra collected by each of the 4 elements of the novel SDD irradiated with a ^{55}Fe radioactive source at an average count rate per channel of about 2 kcps. (Gaussian shaping amplifier with 1 μs shaping time).

4. HIGH-RATE DATA ACQUISITION SYSTEM

The detector signals are read-out with a dedicated high-rate data acquisition system [9]. Figure 6 shows the basic structure of the DAQ. It consists of four main sections: analog, digital, motion control and user interface.

The analog section includes 4 custom designed 5th order pseudo-Gaussian shaping amplifiers with user selectable shaping time (150 ns or 450 ns) and 4 fast amplifiers (30 ns shaping time constant) to provide the trigger signals for the pile-up rejection unit (PUR).

The digital section is based on a field-programmable gate array (FPGA) operating at a maximum clock frequency of 48 MHz. The FPGA controls the data acquisition process and stores the four spectra in the on-chip random access memory (RAM). The amplitudes of the slow shaped pulses are caught by four peak-stretchers and multiplexed into a single signal line, which is sampled by a 10 MSPS 14-bit analog-to-digital converter (ADC).

The motion control section takes care of the automatic scan of the sample area under analysis. It communicates with MM4005 Newport motion controller via the RS232 port. Several tests to verify the performance of the data acquisition system in terms of shaper transfer function, noise performance, and PUR functionality have been carried out and are reported in [8]. The main aim of the experimental characterization that we present in this paper

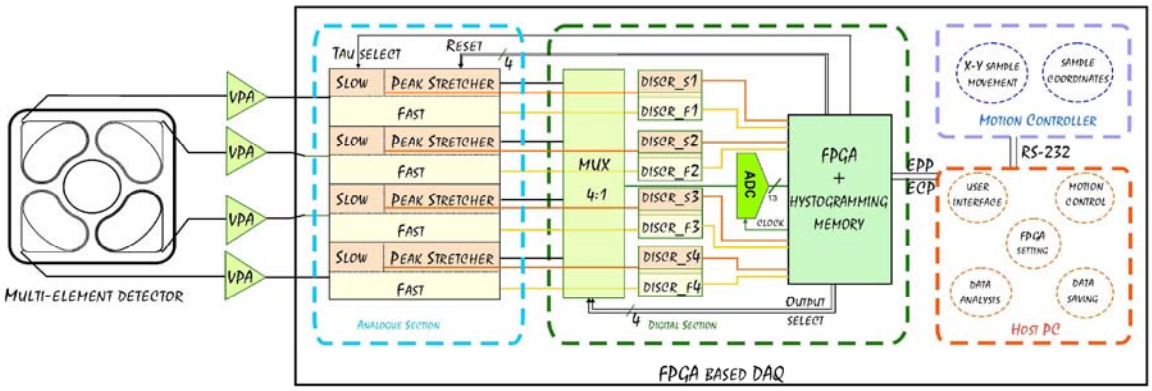

Figure 6. Basic structure of the Data Acquisition System coupled to the 4-channel SDD Droplet ring-detector.

is the assessment of the rate performance. Measurements of the output throughput were performed using a frequency-adjustable random pulse generator (DB2 by Berkley Nucleonics Corporation) connected to the shaping amplifier as well as using the four channel SDD irradiated with a ^{55}Fe source at different detector-source distances. Measurements performed with a frequency-adjustable random pulse generator (DB2 by Berkley Nucleonics Corporation) connected to the shaping amplifier give a maximum throughput of 200 kcps per channel at 450 ns shaping time and of 0.9 Mcps at 150 ns shaping time (with PUR disabled). Similar measurements have been repated also with the detector irradiated with a ^{55}Fe radioactive source at count rates up to 300kcps, limited by the source intensity.

5. EXAMPLES OF ELEMENTAL MAPPING APPLICATION WITH A MICRO-FOCUS X-RAY GENERATOR

5.1. The XRF Spectrometer for elemental mapping

The novel 4-element detector described in Section 3 has been used as the sensing element of a spectrometer for high-resolution fast elemental mapping. A micro-focus X-ray generator, equipped with a W anode and coupled to a polycapillary X-ray lens focuses the primary beam on the sample through the hole laser-cut in the centre of the detector chip. This geometry allows the collection of a large fraction of the fluorescence emitted by the sample and the polycapillary lens concentrates a high photon flux on a small spot on the sample (with a diameter of a few tens of micrometers). Moreover, the distance between the sample and the detector can be reduced with a corresponding reduction of air absorption on the fluorescence of light elements. These features, together with the high detection rate of the SDDs, shorten the scanning time in elemental mapping. A sealed case filled with dry nitrogen and equipped with two beryllium windows houses the detector chip that is cooled by Peltier elements. An X-Y remote-controlled displacement stage is responsible of sample scanning.

In the following we present few examples of the analyses obtained with the new 4-element device installed in the spectrometer in different application fields.

5.2. Analysis of a fossil fish

We studied the distribution of elements in fossils. Fig. 7a shows a photograph of one of the analyzed fossils (Dastilbe Elongatus of Cretaceus Age from Brazil). We scanned an area of 10 mm × 10 mm with 500 μm × 500 μm pitch in the tail region. An acquisition time of 2 s has been accorded to each measurement point and the total measurement time is about 900 s. Figure 7b shows the corresponding map of the iron distribution.

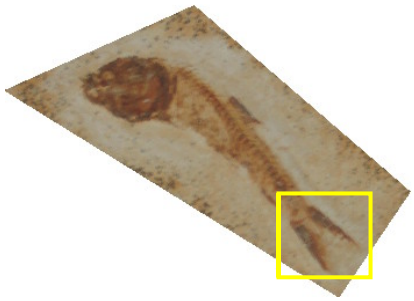

(a)

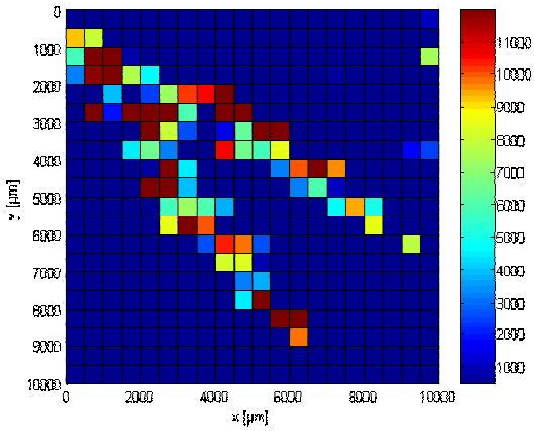

(b)

Figure 7. a) Photograph of the analyzed fossil fish (Dastilbe Elongatus). The scanned area is surrounded with a rectangle. b) Map of the iron distribution (integral of the counts at the Fe Kα line) in the fossil fish tail.

5.3. Analysis of diluted chemical solution

In order to estimate the minimum detection limits of the spectrometer a first set of measurements has been carried out on a solution of iodine in isopropyl alcohol (C_3H_8O) at different dilutions. Figure 8a shows the integral of the counts in the iodine Lα line as a function of the iodine concentration (0.3 ml of solution poured in a 10 mm diameter and 5 mm deep hole in a Lucite phantom). The measurement of each point of the curve lasted 500 s. The minimum level of iodine detected is about 10 μg/ml. Figure 8b shows an example of the acquired spectrum at the two lower probed concentrations.

5.4. Works of art investigation

In cooperation with the Civic Archaeological Museum of Milano a campaign of analyses of Lombard finds of the VII century was performed. Figure 9 shows a Lombard buckle found in a rich grave near Trezzo d'Adda (North of Italy). The result of the elemental mapping analysis of a detail of this inlaid work (agemina) is shown in Figure 10. On the Iron substrate thin strips of Silver and Brass have been inserted by the craftsman in narrow engravings whose transversal dimensions are of the order of some hundreds micrometers. The scanned area is 5mm x 5mm with 250 μm pitch. An acquisition time of 2 s has been accorded to each measurement point. The analyses of other inlaid works found in the same grave show the use also of strips of Gold by the Lombard craftsmen. The composition of the different alloys has been determined too. Table I shows the results for the agemina shown in Figure 9.

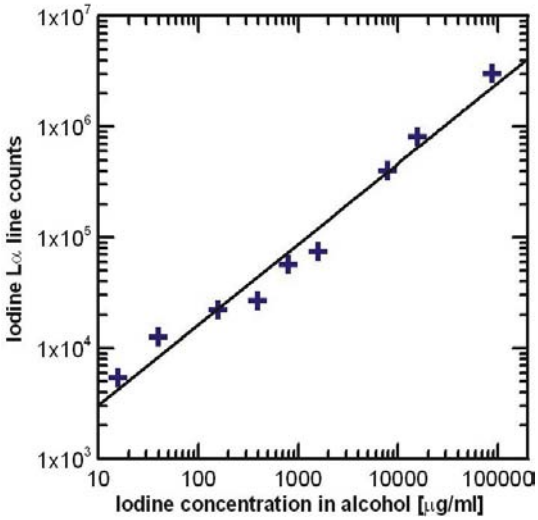

(a)

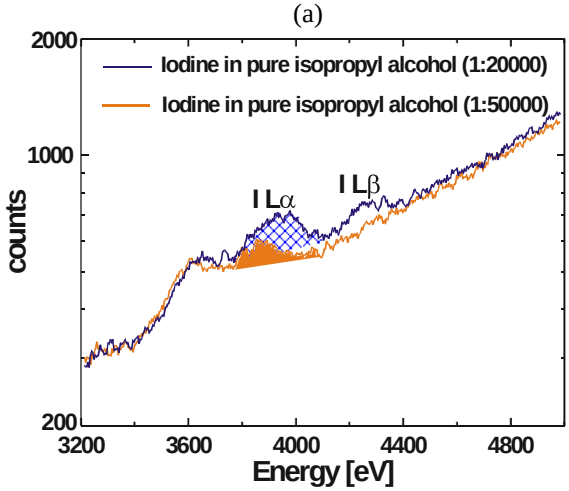

(b)

Figure 8. a) Iodine Lα line intensity (integral of the counts) as a function of the iodine concentration in alcohol. b) Acquired spectrum in the iodine region of interest at the two lower probed concentrations.

Figure 9. Photography of the Lombard buckle analyzed with the spectrometer (Courtesy of the Civico Museo Archeologico di Milano). The analyzed area is highlighted with a square.

Table 1: Element composition of the agemina shown in Figure 9:

Element	Substrate	Silver layer	Brass layer
Iron	91.3%	0.6%	0.8%
Copper	3.5%	11.3%	83.1%
Zinc	1.3%	0.6%	15.2%
Silver	3.45%	87.5%	0.9%

Acknowledgments

The authors would like to thank A. Bjeoumikhov of IfG GmbH, Berlin (Germany) for the policapillary optics, Fabio Bonomelli for his help in the experimental phase, the Museo Archeologico Civico di Milano (L. Miazzo and M. De Marchi) for the analyses of the Lombard manufacts, Sergio Masci for the careful bonding of the detector chip and Luciano Pallaro for the mechanical housing.

Work supported by INFN, Sezione di Milano, FELIX (Fast ELement Imaging with X-ray spectroscopy) experiment.

References

[1] E.Gatti and P.Rehak, "Semiconductor Drift Chamber - An application of a novel Charge Transport Scheme," Nucl. Instr. Meth., vol. A 225, pp. 608-614, 1984.

[2] E. Gatti and P. F. Manfredi, Riv. Nuovo Cimento 9, No. 1 (1986).

[3] P. Lechner, S. Eckbauer, R. Hartmann, S. Krisch, D. Hauff, R. Richter, H. Soltau, L. Strüder, C. Fiorini, E. Gatti, A. Longoni, M. Sampietro,

"Silicon drift detectors for high resolution room temperature X-ray spectroscopy," Nucl. Instr. Meth., vol. A 377, pp. 346-351, 1996.

[4] R.Hartmann, D.Hauff, P.Lechner, R.Richter, L.Strüder, J.Kemmer, S.Krisch, F.Scholze, G.Ulm, "Low energy response of silicon pn-junction detector", Nucl. Instr. and Meth. A 377, 191-196 (1996).

[5] A.Longoni, C.Fiorini, C.Guazzoni, A.Gianoncelli, L.Strüder, H.Soltau, P.Lechner, A.Bjeoumikhov, J.Schmalz, N.Langhoff, R.Wedell, "A new XRF spectrometer based on a ring-shaped multi-element silicon drift detector and on X-ray capillary optics", IEEE Trans. Nucl. Sci., Vol. 49, no.3, June 2002, pp. 1001-1005.

[6] P.Lechner, C.Fiorini, R.Hartmann, J.Kemmer, N.Krause, P.Leutenegger, A.Longoni, H.Soltau, D.Stötter, R.Stötter, L.Strüder, U.Weber, "Silicon drift detectors for high count rate X-ray spectroscopy at room temperature", *Nucl. Instrum. Meth.*, vol. A 458, pp. 281-287, 2001.

[7] A.Longoni, C. Fiorini, C. Guazzoni, S. Buzzetti, M. Bellini, L. Strüder, P. Lechner, A. Bjeoumikov, J. Kemmer, "A novel high resolution XRF spectrometer for elemental mapping based on a monolithic array of Silicon Drift Detectors and on a polycapillary X-ray lens", X-ray Spectrometry, Vol. 34, 2005, pp. 439-445; DOI:10.1002/xrs.858.

[8] A. Longoni, C. Fiorini, C. Guazzoni, S. Buzzetti, M. Bellini, A. Gola, L. Strüder, P. Lechner,A. Bjeoumikov and J. Kemmer, "XRF Spectrometers based on Monolithic Arrays of Silicon Drift Detectors: Elemental Mapping Analyses and Advanced Detector Structures", IEEE Trans. Nucl. Sci., Vol. 53(2), pp. 641 – 647, 2006.

[9] S. Buzzetti, M. Capou, C. Guazzoni, A. Longoni, R. Mariani, S. Moser, " High-speed FPGA-based pulse-height analyzer for high resolution X-ray spectroscopy", IEEE Trans. Nucl. Sci., Vol. 52, no.4, August 2005, pp. 854-860.

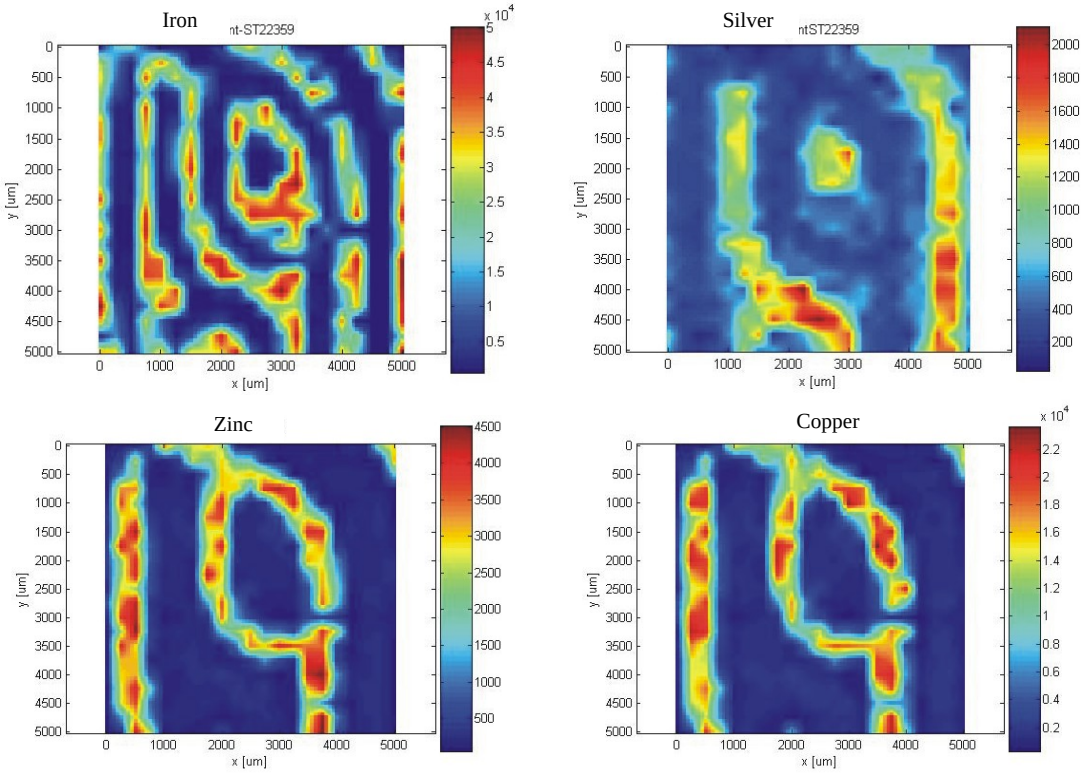

Figure 10. Elemental mapping of the Lombard buckle shown in Figure 9.